

Nanoreactors for Simultaneous Remote Thermal Activation and Optical Monitoring of Chemical Reactions

Carmen Vázquez-Vázquez,[†] Belén Vaz,[‡] Vincenzo Giannini,[§] Moisés Pérez-Lorenzo,^{*,†}
Ramon A. Alvarez-Puebla,^{*,⊥,||} and Miguel A. Correa-Duarte^{*,†}

[†]Department of Physical Chemistry and [‡]Department of Organic Chemistry, Universidade de Vigo, 36310 Vigo, Spain

[§]Department of Physics, Imperial College London, London SW7 2AZ, U.K.

[⊥]Universitat Rovira i Virgili and Centro de Tecnologia Química de Catalunya, Carrer de Marcel·lí Domingo s/n, 43007 Tarragona, Spain

^{||}ICREA, Passeig Lluís Companys 23, 08010 Barcelona, Spain

S Supporting Information

ABSTRACT: We report herein the design of plasmonic hollow nanoreactors capable of concentrating light at the nanometer scale for the simultaneous performance and optical monitoring of thermally activated reactions. These reactors feature the encapsulation of plasmonic nanoparticles on the inner walls of a mesoporous silica capsule. A Diels–Alder cycloaddition reaction was carried out in the inner cavities of these nanoreactors to evidence their efficacy. Thus, it is demonstrated that reactions can be accomplished in a confined volume without alteration of the temperature of the bulk solvent while allowing real-time monitoring of the reaction progress.

The unprecedented ability of plasmon-resonant metallic structures to concentrate light at the nanometer scale^{1,2} has propelled their use in a vast array of photonics technologies (plasmonics) and research endeavors. Together with the electromagnetic near field generated upon exposure of the metallic nanostructures to the appropriate light (i.e., localized surface plasmon resonances, LSPRs),^{3,4} the intense optical absorption at the surface plasmon resonance frequency is also responsible for strong heat generation through an efficient light–heat conversion.^{5–7} This effect has recently opened multiple opportunities, such as photothermal therapy,⁸ drug delivery,⁹ and fluid motion control.¹⁰ Interestingly, by controlling the size, shape, composition, and structure of the plasmonic structures, it is possible to maximize these effects (heating and sensing) in certain regions of a whole volume while preserving the rest unaltered. This precise control gives rise to the possibility of performing heat-activated reactions and simultaneous optical monitoring in temperature-sensitive media such as biological environments. Plasmon-assisted sensing processes offer exceptional possibilities,¹¹ as in the case of catalytic reactions.¹² Nevertheless, only a few approaches combining chemistry, material science, and optics have been addressed so far for the development of plasmonic probes for catalytic reactions that can operate under realistic conditions. Among them, antenna-enhanced hydrogen sensors at the single-particle level were designed by placing a palladium particle close to the tip of a gold nanoantenna and then

measuring the shift in the scattered spectrum.¹³ Following a different strategy, changes in surface coverage of reactants along the progress of various catalytic transformations were monitored through optical spectroscopy, with the catalyst supported on gold nanodisk arrays.¹⁴

We report herein the design, fabrication, and application of plasmonic nanoreactors (PNRs) for the simultaneous performance and monitoring of thermally induced confined chemical processes (Figure 1). These PNRs function as heat nanosources

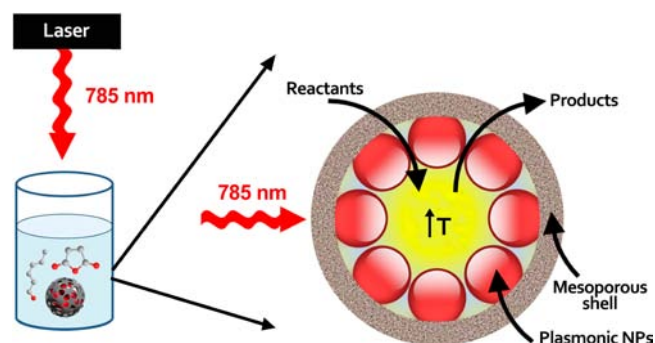


Figure 1. Schematic cross-section view of the PNR developed in this work where reactants and products diffuse through the mesoporous silica shell and NIR laser irradiation promotes the chemical reaction, allowing simultaneous *in situ* SERS monitoring of the process.

upon external illumination, promoting the conversion of reactants into products. These systems allow specifically activating the confined volume while avoiding temperature alterations within the bulk solution. Furthermore, since the thermal effect is induced by the excitation of the LSPR inside the reactors, the electromagnetic field generated can be exploited for *in situ* surface-enhanced Raman spectroscopy (SERS) monitoring of the process.

Preparation of the nanoreactors requires a special type of hollow capsules based on inorganic porous membranes that encapsulate plasmonic nanoparticles (NPs) in optimized configurations.^{15,16} Given the high permeability of mesoporous

Received: May 23, 2013

Published: August 29, 2013

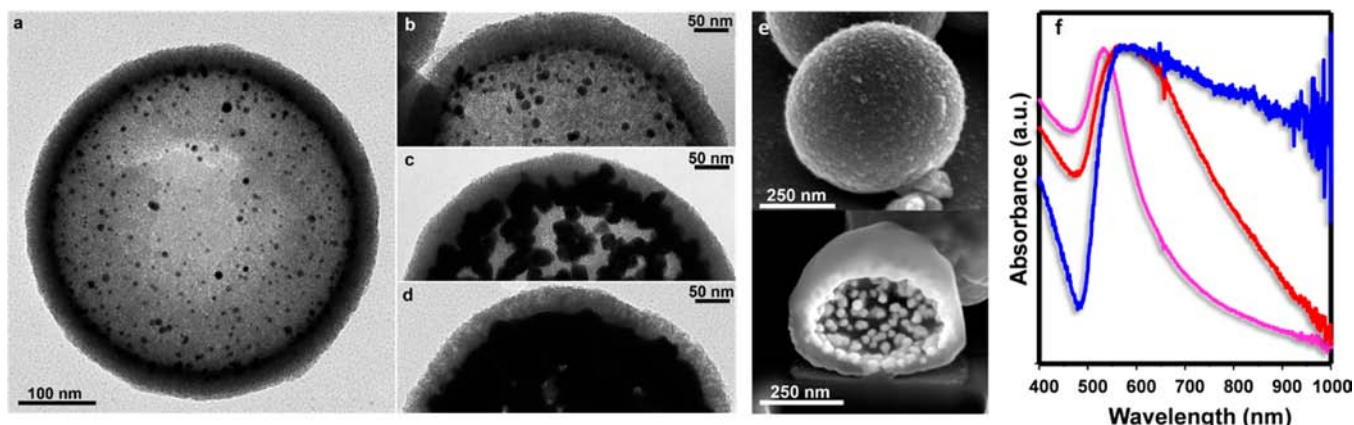


Figure 2. Typical TEM images of the PNRs (a,b) before and (c,d) after the controlled growth of the inner AuNPs. (e) SEM images of a complete capsule and after slicing with a focused ion beam to observe the AuNPs on the inner silica wall. (f) Localized surface plasmon resonances of capsules as prepared (pink) and after the two sequential overgrowths (red and blue).

silica, this material was selected as an appropriate shell allowing an effective exchange of reactants between the inner cavity and the bulk solution.¹⁷ Likewise, its thermal insulation capacity constitutes an additional advantage.¹⁸

The Au seeds (2–3 nm) were first deposited onto 550 nm positively charged polystyrene particles, obtained through electrostatic layer-by-layer self-assembly.¹⁶ After that, the polystyrene@Au particles were coated with a homogeneous mesoporous silica layer by using tetraethoxysilane in ethanol.¹⁹ The polymeric core was then removed by calcination (550 °C, 8 h) (see experimental details in the Supporting Information). Figure 2a,b shows transmission electron microscopy (TEM) images of the as-prepared nanoreactors after calcination. These images clearly illustrate the silica shell and the individual Au seeds in their inner cavity. The gold seeds can be selectively overgrown by a catalyzed epitaxial reduction of gold ions with formaldehyde (Figure 2c,d). STEM and XEDS (Figure S1) provide further evidence on the exclusive AuNPs growth in the inner space of the silica capsule, as no trace of gold was detected on the outer surface. Additionally, the focused ion beam cross-section analysis of the PNRs confirms the morphological configuration of plasmonic NPs supported on the inner walls of the mesoporous shell (Figure 2e). This controlled growth represents a unique strategy that allows optimizing the optical properties of the plasmonic reactor for both plasmonic-assisted heating and SERS sensing. Figure 2f shows how the LSPRs red-shift and broaden as the particles increase in size, demonstrating an efficient plasmon coupling and, thus, the formation of hot spots (1 mg/mL capsule dispersions).

In order to test the optical efficiency for SERS and to evidence the molecular transport through the mesoporous shell (as a measure of the porosity), we designed an experiment comprising three SERS probes with considerably different molecular areas. Figure S2 shows the molecular structures and dimensions, the SERS spectra, and the retention kinetics of benzenethiol (BT), crystal violet (CV), and (5''-(4'-(methylthio)-[1,1'-biphenyl]-4-yl)-[1,1':4',1'':3'',1''':4''',1''''-quinquephenyl]-4,4''''-diyl)bis(methylsulfane) (3S) on the AuNPs. Although these three compounds yield strong SERS signals, the adsorption rate of the probes on the gold surfaces decreases with molecular size as a consequence of the pore size restriction of the silica wall. Notwithstanding, this test clearly demon-

strates the diffusion of considerably large molecular systems (up to 2.5 nm) through the capsule shell.

The temperature variation inside the capsule upon illumination with near-infrared (NIR) light (785 nm) can be estimated through theoretical modeling by the numerical solution of the Poisson equations in a model material (Figure S3).²⁰ The nanoreactors are simulated considering a silica shell with a diameter of 550 nm and thickness of 30 nm, covered in its internal surface with a layer of spherical AuNPs with a diameter of 40 nm and an average gap of 4 nm. In the nanoreactor, the inner AuNPs are the unique thermal sources. Since their thermal conductivity ($\kappa_{\text{gold}} = 318 \text{ W m}^{-1} \text{ K}^{-1}$) is also far larger than those of the other components ($\kappa_{\text{solvent}} = 0.6 \text{ W m}^{-1} \text{ K}^{-1}$, $\kappa_{\text{silica}} = 0.05 \text{ W m}^{-1} \text{ K}^{-1}$),²¹ we can consider the temperature uniform for the AuNPs.²² These calculations show that, while the temperature inside the reactor increases 90 °C, thermal heating of the exterior bulk solution is almost inhibited. Nonetheless, although the conduction heat transfer is hindered by the insulating silica shell, the convective transfer due to the mesoporous nature of the shell is favored by the generation of a thermal gradient between the interior and the solution, which, in turn, may facilitate the diffusion of reactants to the nanoreactors and the products to the bulk solution.

As a proof of concept, given its wide use in synthetic organic chemistry and its pivotal importance as an atom-economic process, Diels–Alder cycloaddition was performed in the presence of the nanocapsules in order to assess their efficacy as nanoreactors. The Diels–Alder reaction consists of an interaction between a 1,3-diene and an alkene (also referred to as a dienophile) to yield a cyclohexene-type structure. The alkene is usually substituted by one or more electron-withdrawing groups, while the diene may be substituted with electron donors. In the absence of these groups, the reaction rates are much slower and require heating. In our approach, 2,4-hexadienol (diene) and maleic anhydride (dienophile) (Figure S4a) were added to a reaction vessel containing a colloidal dispersion of capsules.

Equimolar concentrations (0.25 M) of the two reactants were used at room temperature. Upon illumination of the solution with a NIR laser, the plasmonic assemblies absorb radiation and dissipate heat as a competitive mechanism that governs the temperature distribution in metallic nanostructures. Thus, in close proximity of the nanometallic surface, the hot surfaces promote the chemical reaction inside the hollow cavity,

ending with the formation of 4-isobenzofurancarboxylic acid. Simultaneously, the same laser source is used to monitor the progress of the reaction. SERS spectroscopy (Figure S4b) shows the spectrum of the maleic anhydride, characterized by strong signals at 1844 cm^{-1} assigned to the C=O stretching in anhydrides ($\text{O}=\text{C}-\text{O}-\text{C}=\text{O}$) and at 1660 cm^{-1} attributed to the C=C stretching of ene bonds coupled to a carbonyl group ($\text{C}=\text{C}-\text{C}=\text{O}$). Notably, no signal in the spectra can be ascribed to either the diene or the product due to their aliphatic nature with the subsequent low SERS cross sections.²³ SERS monitoring of these two bands shows a consistent decrease in their intensity over time, due to the formation of the product with complete disappearance of the reactant after 45 min (Figure 3a,b). It is worth noting that the temperature of

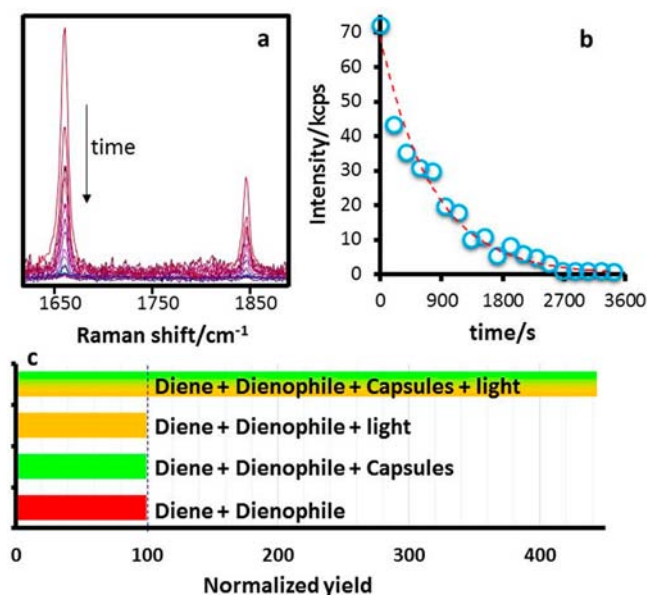


Figure 3. (a,b) SERS monitoring of the reaction occurring inside the nanocapsule over the time. (c) Comparison of the reaction yields after 30 min determined by ^1H NMR for our system and controls including the diene and dienophile in the presence and absence of capsules and light (see Figure S5 for further details).

the bulk solution remained fairly constant over the entire process. In order to compare our results with other experimental configurations, the same reaction was carried out with capsules without light, with light without capsules present, and in the absence of both capsules (and therefore, the AuNPs contained therein) and light. As shown in Figure 3c, there is a remarkable increase in the reaction yield when the cycloaddition reaction is performed in the presence of capsules under laser irradiation. As observed, this improvement in the reaction efficiency cannot be justified on the basis of a mere catalytic effect due to the AuNPs or a laser-induced cyclization. Not even the moderate increase ($+8\text{ }^\circ\text{C}$) in the sample temperature resulting from the heat dissipation of the AuNPs through the isolating silica shell is enough to explain this acceleration in the cycloaddition rate. Thus, by discounting the effect of the temperature rising, a $\sim 300\%$ increase in the reaction yield is still found. This observation points to a Diels–Alder cycloaddition taking place at a much higher temperature than that measured for the bulk solvent.

In summary, we have described the preparation of plasmonic nanoreactors and their use to trigger thermally activated

reactions in confined volumes without alteration of the temperature of the bulk solvent. This could be of special relevance in applications involving biological environments. Additionally, these reactors can be used for real-time monitoring of the process, providing an alternative to collect real-time information about the course of chemical reactions, critical indeed for the improvement of relevant chemical processes.

■ ASSOCIATED CONTENT

📄 Supporting Information

Experimental procedures and theoretical methods. This material is available free of charge via the Internet at <http://pubs.acs.org>.

■ AUTHOR INFORMATION

Corresponding Authors

moisespl@uvigo.es
ramon.alvarez@urv.cat
macorrea@uvigo.es

Notes

The authors declare no competing financial interest.

■ ACKNOWLEDGMENTS

B.V. and M.P.-L acknowledge financial support from Isidro Parga Pondal Program. This work was funded by the Spanish Ministerio de Economía y Competitividad (CTQ2011-23167), the European Research Council (CrossSERS, FP7MC-IEF 329131, and METACHEM, grant no. CP-FP 228762-2), Xunta de Galicia (INBIOMED-FEDER “unha maneira de facer Europa”), and Fundación Ramón Areces.

■ REFERENCES

- Alvarez-Puebla, R.; Liz-Marzán, L. M.; García de Abajo, F. J. *J. Phys. Chem. Lett.* **2010**, *1*, 2428.
- Schuller, J. A.; Barnard, E. S.; Cai, W.; Jun, Y. C.; White, J. S.; Brongersma, M. L. *Nat. Mater.* **2010**, *9*, 193.
- Atwater, H. A.; Polman, A. *Nat. Mater.* **2010**, *9*, 205.
- Lal, S.; Link, S.; Halas, N. J. *Nat. Photon.* **2007**, *1*, 641.
- Adleman, J. R.; Boyd, D. A.; Goodwin, D. G.; Psaltis, D. *Nano Lett.* **2009**, *9*, 4417.
- Sanchot, A.; Baffou, G.; Marty, R.; Arbouet, A.; Quidant, R.; Girard, C.; Dujardin, E. *ACS Nano* **2012**, *6*, 3434.
- Baffou, G.; Quidant, R. *Laser Photon. Rev.* **2013**, *7*, 171.
- Bardhan, R.; Lal, S.; Joshi, A.; Halas, N. J. *Acc. Chem. Res.* **2011**, *44*, 936.
- Huschka, R.; Zuloaga, J.; Knight, M. W.; Brown, L. V.; Nordlander, P.; Halas, N. J. *J. Am. Chem. Soc.* **2011**, *133*, 12247.
- Donner, J. S.; Baffou, G.; McCloskey, D.; Quidant, R. *ACS Nano* **2011**, *5*, 5457.
- Li, J. F.; Huang, Y. F.; Ding, Y.; Yang, Z. L.; Li, S. B.; Zhou, X. S.; Fan, F. R.; Zhang, W.; Zhou, Z. Y.; WuDe, Y.; Ren, B.; Wang, Z. L.; Tian, Z. Q. *Nature* **2010**, *464*, 392.
- Tittel, A.; Yin, X.; Giessen, H.; Tian, X.-D.; Tian, Z.-Q.; Kremers, C.; Chigrin, D. N.; Liu, N. *Nano Lett.* **2013**, *13*, 1816.
- Liu, N.; Tang, M. L.; Hentschel, M.; Giessen, H.; Alivisatos, A. P. *Nat. Mater.* **2011**, *10*, 631.
- Larsson, E. M.; Langhammer, C.; Zorić, I.; Kasemo, B. *Science* **2009**, *326*, 1091.
- Sanles-Sobrido, M.; Pérez-Lorenzo, M.; Rodríguez-Gonzalez, B.; Salgueirino, V.; Correa-Duarte, M. A. *Angew. Chem., Int. Ed.* **2012**, *51*, 3877.
- Sanles-Sobrido, M.; Exner, W.; Rodríguez-Lorenzo, L.; Rodríguez-Gonzalez, B.; Correa-Duarte, M. A.; Alvarez-Puebla, R. A.; Liz-Marzán, L. M. *J. Am. Chem. Soc.* **2009**, *131*, 2699.

- (17) Chen, Z.; Cui, Z.-M.; Niu, F.; Jiang, L.; Song, W.-G. *Chem. Commun.* **2010**, 46, 6524.
- (18) Yue, Q.; Li, Y.; Kong, M.; Huang, J.; Zhao, X.; Liu, J.; Williford, R. E. *J. Mater. Chem.* **2011**, 21, 12041.
- (19) Deng, Y.; Qi, D.; Deng, C.; Zhang, X.; Zhao, D. *J. Am. Chem. Soc.* **2008**, 130, 28.
- (20) Baffou, G.; Girard, C.; Quidant, R. *Phys. Rev. Lett.* **2010**, 104, 136805.
- (21) Dong, D.; Xue, W.; Liu, X.; He, W.; Hu, W. *Microporous Mesoporous Mater.* **2011**, 143, 54.
- (22) Baffou, G.; Quidant, R.; García de Abajo, F. J. *ACS Nano* **2010**, 4, 709.
- (23) Alvarez-Puebla, R. A.; Liz-Marzán, L. M. *Angew. Chem., Int. Ed.* **2012**, 51, 11214.